

# Supplementary Material of “Constructing High-order Functional Connectivity Networks with Temporal Information from fMRI Data”

Yingzhi Teng, Kai Wu, *Member, IEEE*, Jing Liu, *Senior Member, IEEE*, Yifan Li, Xiangyi Teng

## I. DATASET

*Resting-state classified fMRI I* are publicly available at the OpenNeuro project: <https://openneuro.org/datasets/ds003548>.

*Resting-state classified fMRI II* are publicly available at the OpenNeuro project: <https://openneuro.org/datasets/ds004349>.

*Alzheimer’s diseases fMRI data* are obtained from The Alzheimer’s Disease Neuroimaging Initiative: [adni.loni.usc.edu](http://adni.loni.usc.edu).

*Reading Brain L1 Adult data* are publicly available at the Reading Brain project: <https://blclab.org/reading-brain>.

## II. DATA PREPROCESSING

We need to preprocess the original functional images and extract the fMRI time series of ROIs. fMRI data are preprocessed using Data Processing Assistant for Resting-State fMRI package [1] (DPARSF)<sup>1</sup>. The steps are as given follows: 1) Slice timing: the initial 10 time points are removed, and the slice-timing correction is performed; 2) Realign: the subjects with head motion exceeding 2.5 mm and 2.5 degrees are excluded; 3) Co-registered: the functional images are co-registered to the T1-weighted structural images, which are further segmented into gray matter, white matter, and cerebrospinal fluid by the segmentation method in SPM<sup>2</sup>; 4) Normalized: the functional images are normalized into the Montreal Neurological Institute (MNI) space by the Diffeomorphic Anatomical Registration Through Exponentiated Lie algebra (DARTEL); 5) Smooth: to reduce the uncertainty of the co-registered, the functional images are smoothed by a 4mm full width at half maximum (FWHM) Gaussian kernel; 6) Filter: functional time series are band-pass filtered at 0.01–0.1 Hz.

TABLE S1  
ALZHEIMER’S DISEASE FMRI DATA CHARACTERISTICS

Characteristics	CN( <i>n</i> =51)	AD( <i>n</i> =51)
Age(years)	73.74 ± 4.80	72.92 ± 5.37
Gender(male/female)	30/21	22/29

<sup>1</sup><http://rfmri.org/DPARSF>

<sup>2</sup><http://www.fil.ion.ucl.ac.uk/spm>

## III. COMPETITIVE METHODS

PC: Pearson’s correlation (PC) is widely used in neuroimaging [2], [3]. PC is used to construct FCNs, and SVM is used for classification.

Lasso-HCC [4]: Lasso regression is used to build the hypergraph, HCC is used as high-order features, and finally, the multi-kernel SVM [5] is used for classification.

UW-ElasticNet and UW-Lasso [6]: Elastic net and Lasso regression are used to build unweighted hypergraphs separately. Node degree, centrality degree, and efficiency are used as the classification features of SVM.

HL [7]: Sparse linear regression is used to construct the hypergraph, and the weights of the hypergraph are obtained by manifold learning. Finally, the similarity matrix is calculated according to the weights as the features for SVM classification.

sgLasso-COMHCC [8]: Spare group Lasso is used to build the hypergraph, HCC and COMHCC are used as high-order features, and finally, the multi-kernel SVM is used for classification.

WHyper-BNM [9]: Lasso is used to build the hypergraph, HCC, and other brain network measures (i.e., Characteristic path length, Local efficiency, and Global efficiency) are used as high-order features. The decision tree based on Gini impurity is used to classify resting-state EEG data.

Lasso-FCM [10]: FCM is constructed using lasso regression and dynamics of Eq. (3) in the main text, and then FCMs are used as data features for SVM classification. Lasso-FCM can reconstruct large-scale gene regulatory networks due to its sparsity.

ElasticNet-HFCM [11]: High-order FCM (HFCM) is constructed using the elastic net and high-order dynamic formula [12], and the predicted values of HFCM are used as features for SVM classification. ElasticNet-HFCM is used to classify EEG data and has competitive performance.

## IV. EXPERIMENTAL SETUP AND PERFORMANCE MEASURES

Standard measures, including accuracy (ACC), sensitivity (SEN), specificity (SPE), F1 Score, and area under the receiver operating characteristic (ROC) curve (AUC), are used to evaluate the classification performance of different methods. The specific formula is defined as follows:

$$ACC = \frac{TP + TN}{TP + FN + TN + FP} \quad (1)$$

$$SEN = \frac{TP}{TP + FN}$$

$$SPE = \frac{TN}{TN + FP}$$

$$F1\ Score = 2 \times \frac{Precision \times Recall}{Precision + Recall}$$

where

$$Precision = \frac{TP}{TP + FP}$$

$$Recall = SEN = \frac{TP}{TP + FN}$$

In resting-state classified fMRI II, Alzheimer's disease data and Reading Brain L1 Adult data, a 5-fold crossover strategy is adopted. Specifically, all the subject samples are divided into 5 groups, and 4 groups are randomly selected for training and the remaining group for testing. The above process is repeated 5 times to avoid bias caused by the partition. In resting-state classified fMRI I, the leave-one-out (LOO) cross-validation is adopted due to the limitation of the number of subjects. Specifically, similar to the 5-fold crossover, one subject is first left out for testing, and the remaining subjects are for training. The process is repeated for each subject.

## REFERENCES

- [1] C. G. Yan, X. D. Wang, X. N. Zuo, and Y. F. Zang, "DPABI: data processing & analysis for (resting-state) brain imaging," *Neuroinformatics*, vol. 14, pp. 339–351, 2016.
- [2] C.-Y. Wee, P.-T. Yap, D. Zhang, K. Denny, J. N. Browndyke, G. G. Potteret, K. A. Welsh-Bohmer, L. Wang, and D. Shen, "Identification of MCI individuals using structural and functional connectivity networks," *NeuroImage*, vol. 59, no. 3, pp. 2045–2056, 2012.
- [3] R. Kashyap, R. Kong, S. Bhattacharjee, J. Li, J. Zhou, and B.-T. Thomas Yeo, "Individual-specific fMRI-Subspaces improve functional connectivity prediction of behavior," *NeuroImage*, vol. 189, pp. 804–812, 2019.
- [4] B. Jie, C.-Y. Wee, D. Shen, and D. Zhang, "Hyper-connectivity of functional networks for brain disease diagnosis," *Medical Image Analysis*, vol. 32, pp. 84–100, 2016.
- [5] F. R. Bach, G. R. Lanckriet, and M. I. Jordan, "Multiple kernel learning, conic duality, and the SMO algorithm," In: *Proceedings of the Twenty-first International Conference on Machine Learning*, 2004.
- [6] H. Guo, Y. Li, Y. Xu, Y. Jin, J. Xiang, and J. Chen, "Resting-state brain functional hyper-network construction based on elastic net and group lasso methods," *Frontiers in Neuroinformatics*, vol. 12, no. 25, 2018.
- [7] L. Xiao, J. Wang, P. H. Kassani, Y. Zhang, Y. Bai, J. M. Stephen, T. W. Wilson, V. D. Calhoun, and Y.-P. Wang, "Multi-hypergraph learning-based brain functional connectivity analysis in fMRI data," *IEEE Transactions on Medical Imaging*, vol. 39, no. 5, pp. 1746–1758, 2019.
- [8] Y. Li, C. Sun, P. Li, Y. Zhao, G. K. Mensah, Y. Xu, H. Guo, and J. Chen, "Hypernetwork construction and feature fusion analysis based on sparse group lasso method on fMRI dataset," *Frontiers in Neuroscience*, vol. 14, no. 60, 2020.
- [9] X. Shao, W. Kong, S. Sun, N. Li, X. Li, and B. Hu, "Analysis of functional connectivity in depression based on a weighted hyper-network method," *Journal of Neural Engineering*, 2023, 10.1088/1741-2552/acb088.
- [10] K. Wu and J. Liu, "Robust learning of large-scale fuzzy cognitive maps via the lasso from noisy time series," *Knowledge-Based Systems*, vol. 113, pp. 23–38, 2016.
- [11] F. Shen, J. Liu, and K. Wu, "Multivariate time series forecasting based on elastic net and high-order fuzzy cognitive maps: a case study on human action prediction through EEG signals," *IEEE Transactions on Fuzzy Systems*, vol. 29, no. 8, pp. 2336–2348, 2020.
- [12] S. Yang and J. Liu, "Time-series forecasting based on high-order fuzzy cognitive maps and wavelet transform," *IEEE Transactions on Fuzzy Systems*, vol. 26, no. 6, pp. 3391–3402, 2018.
- [13] A. Khazaee, A. Ebrahimpour, A. Babajani-Feremi, and Alzheimer's Disease Neuroimaging Initiative, "Time-series forecasting based on high-order fuzzy cognitive maps and wavelet transform," *Behavioural Brain Research*, vol. 322, pp. 339–350, 2017.

TABLE S2

COMPARISON OF CLASSIFICATION PERFORMANCE OF THFCN WITH ITS VARIANTS ON RESTING-STATE CLASSIFIED FMRI I DATA.

Method	ACC	SEN	SPE	F1 Score	AUC
THFCN w/o TI	0.8621	1.0000	0.6923	0.8889	0.8462
THFCN w/o hyper	0.9310	1.0000	0.8462	0.9412	0.9231
<b>THFCN</b>	<b>0.9655</b>	<b>1.0000</b>	<b>0.9231</b>	<b>0.9697</b>	<b>0.9615</b>

TABLE S3

COMPARISON OF CLASSIFICATION PERFORMANCE OF THFCN WITH ITS VARIANTS ON RESTING-STATE CLASSIFIED FMRI II DATA.

Method	ACC	SEN	SPE	F1 Score	AUC
THFCN w/o TI	$0.7791 \pm 0.1010$	$0.8583 \pm 0.0889$	$0.7028 \pm 0.1833$	$0.7975 \pm 0.0869$	$0.8389 \pm 0.1099$
THFCN w/o hyper	$0.6621 \pm 0.0711$	$0.8333 \pm 0.1258$	$0.4889 \pm 0.0893$	$0.7074 \pm 0.0808$	$0.4694 \pm 0.1059$
<b>THFCN</b>	<b><math>0.9765 \pm 0.0288</math></b>	<b><math>1.0000 \pm 0.0000</math></b>	<b><math>0.9527 \pm 0.0580</math></b>	<b><math>0.9777 \pm 0.0274</math></b>	<b><math>0.9972 \pm 0.0056</math></b>

TABLE S4

COMPARISON OF CLASSIFICATION PERFORMANCE (MEAN $\pm$ STD) OF THFCN WITH ITS VARIANTS ON ALZHEIMER'S DISEASE FMRI DATA.

Method	ACC	SEN	SPE	F1 Score	AUC
THFCN w/o TI	$0.5250 \pm 0.0847$	$0.5000 \pm 0.1767$	$0.5500 \pm 0.2031$	$0.5000 \pm 0.1196$	$0.5438 \pm 0.1301$
THFCN w/o hyper	$0.7125 \pm 0.0847$	$0.6250 \pm 0.1581$	$0.8000 \pm 0.1695$	$0.6792 \pm 0.1046$	$0.6938 \pm 0.0991$
<b>THFCN</b>	<b><math>0.7500 \pm 0.1046</math></b>	<b><math>0.6750 \pm 0.1500</math></b>	<b><math>0.8250 \pm 0.1870</math></b>	<b><math>0.7276 \pm 0.1188</math></b>	<b><math>0.7031 \pm 0.1022</math></b>

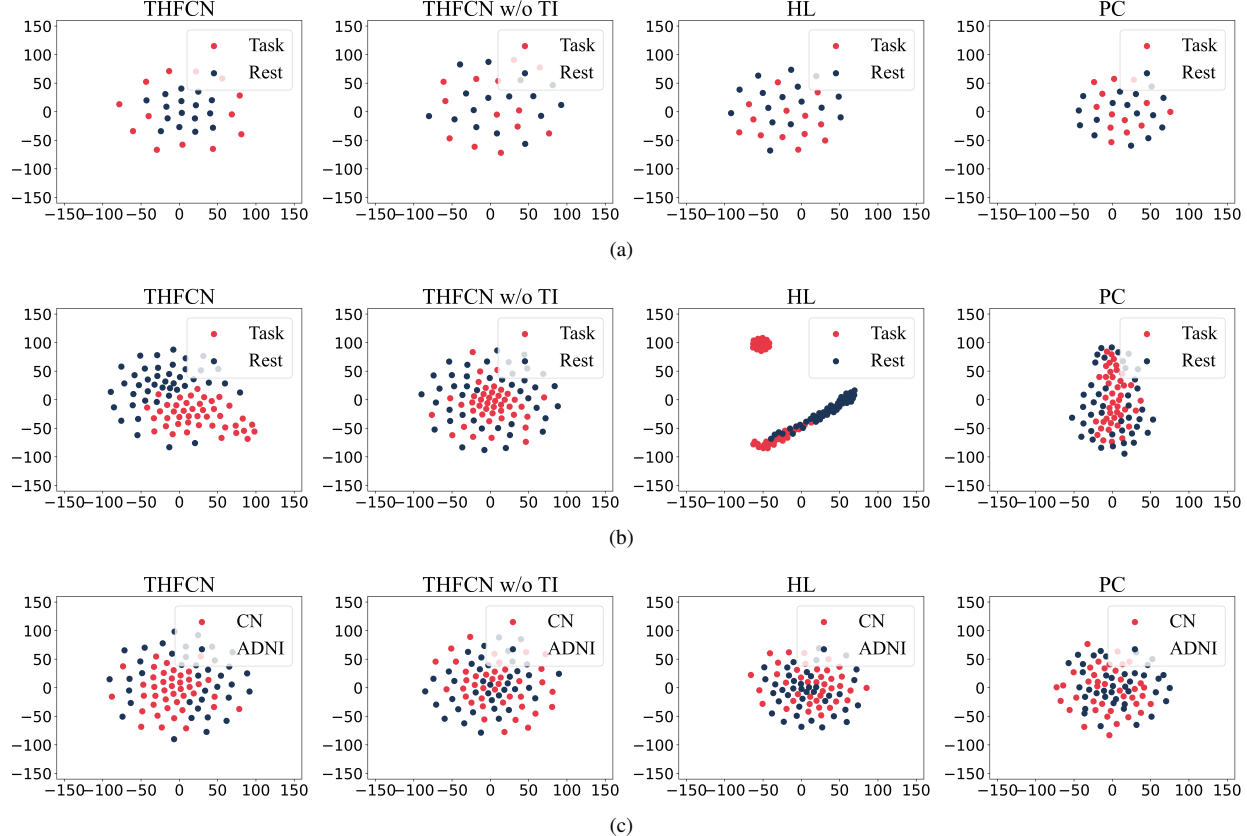
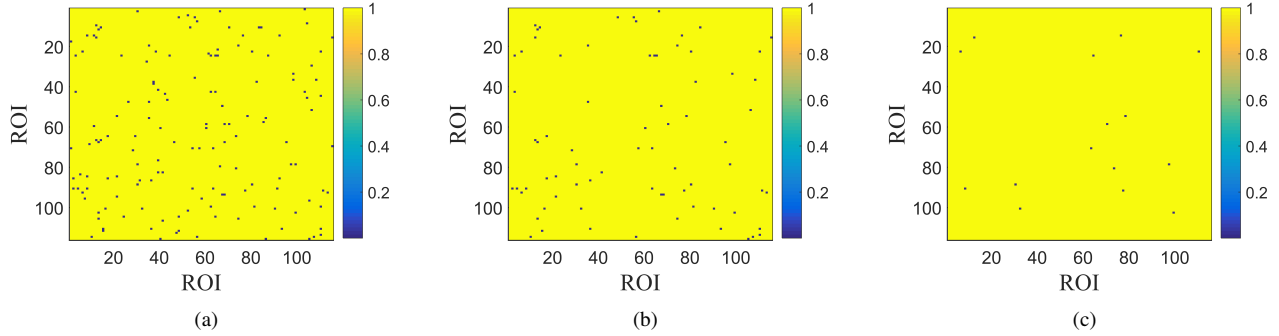
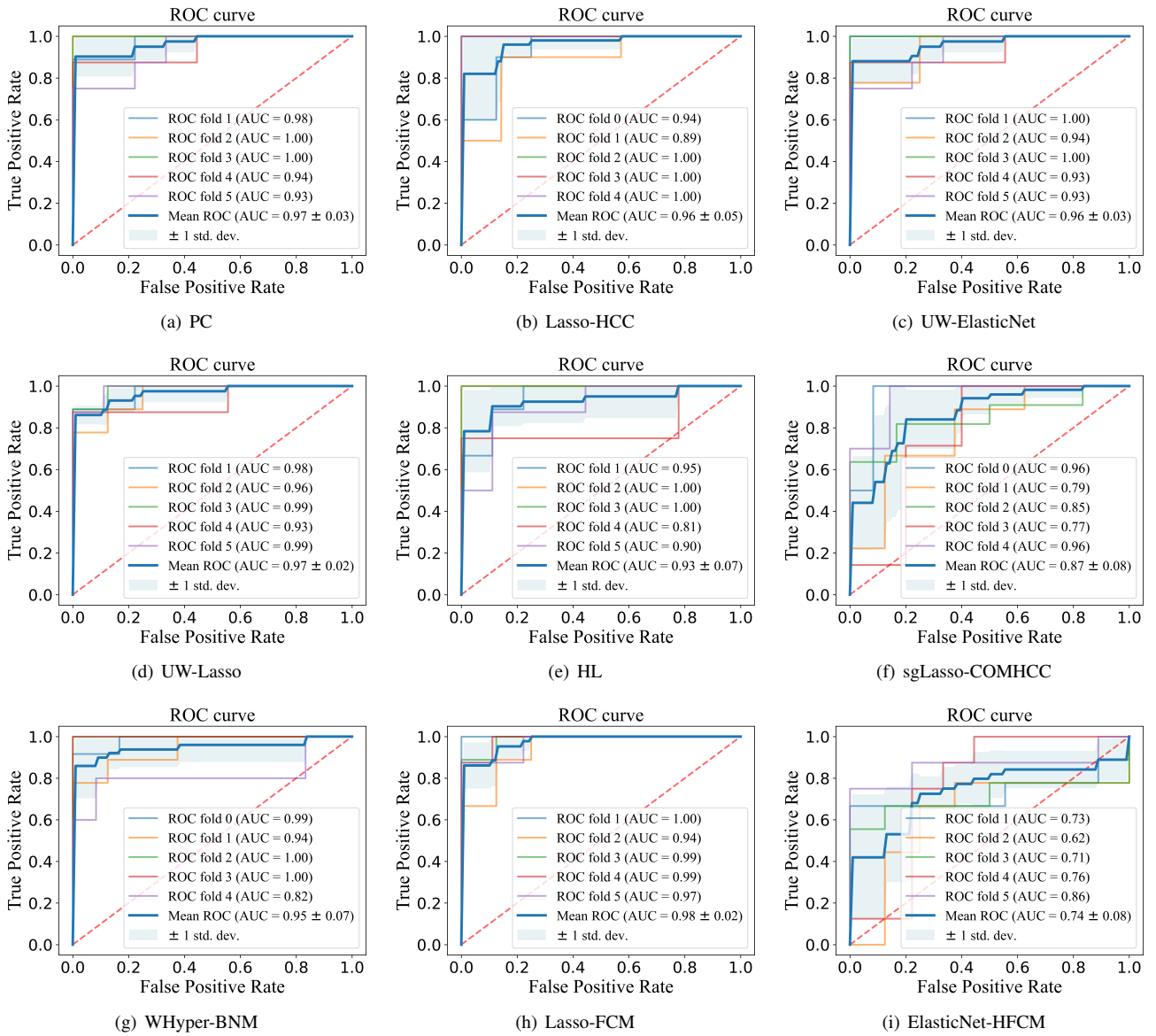
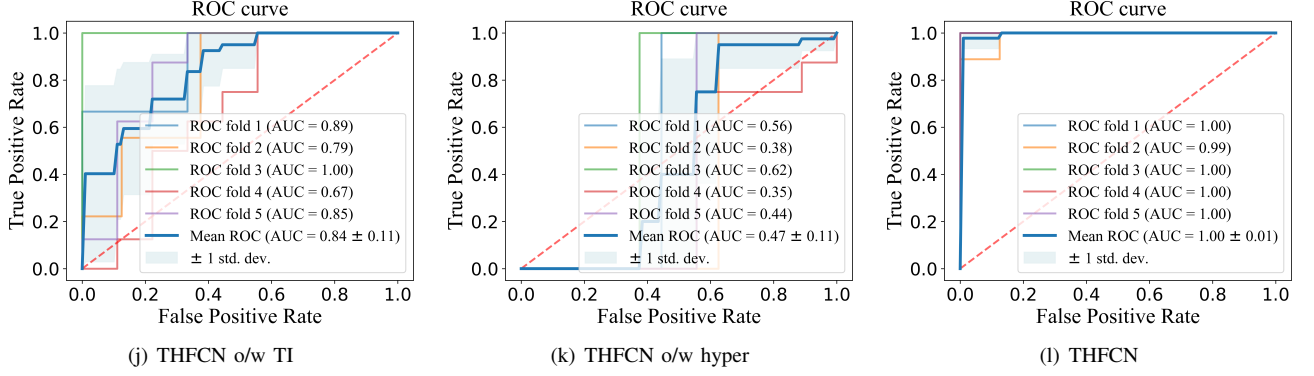


Fig. S1. t-SNE visualization of THFCN with non-temporal baselines on three fMRI datasets, including (a) resting-state classified fMRI I, (b) resting-state classified fMRI II, and (c) Alzheimer's disease fMRI data.

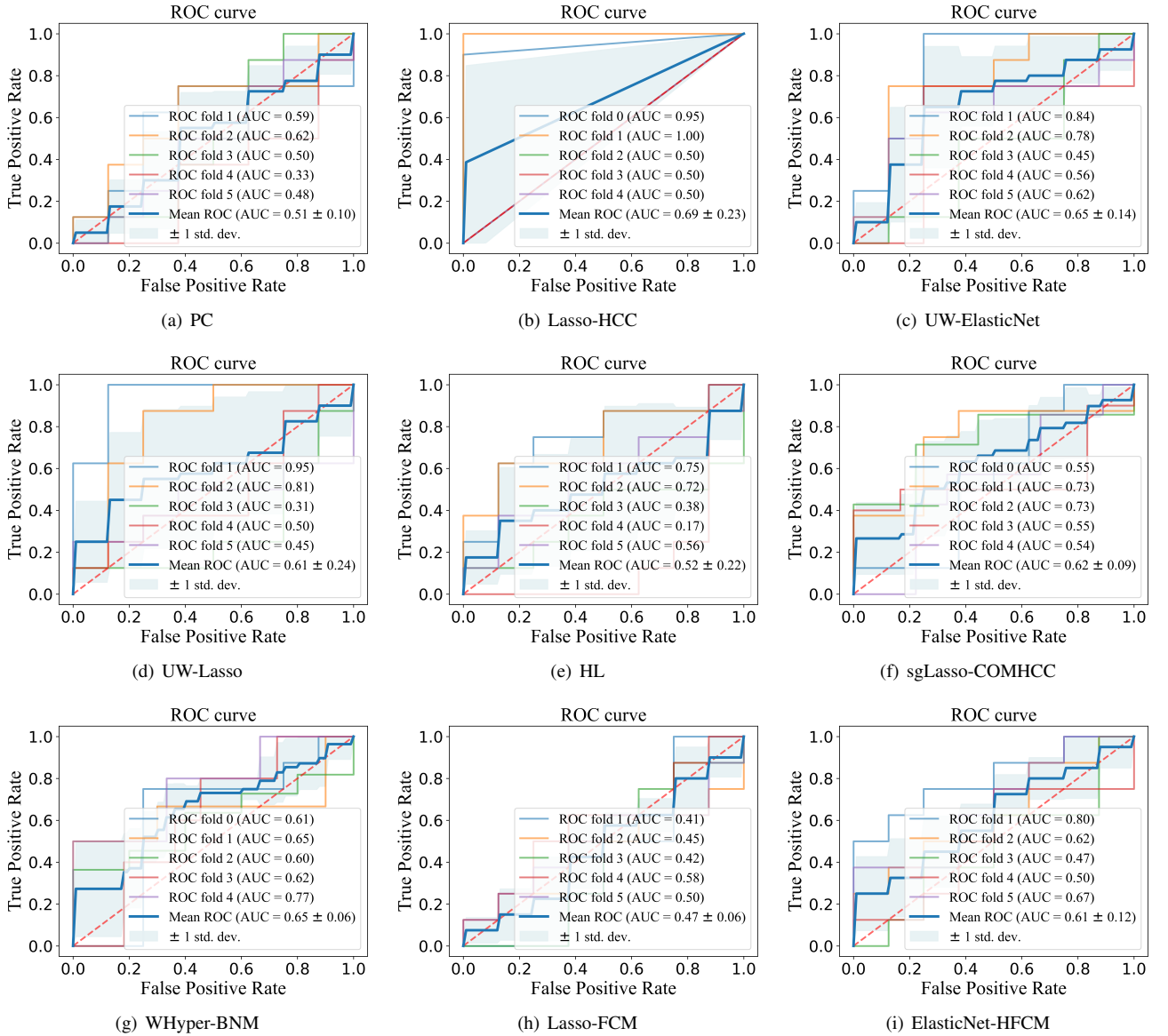


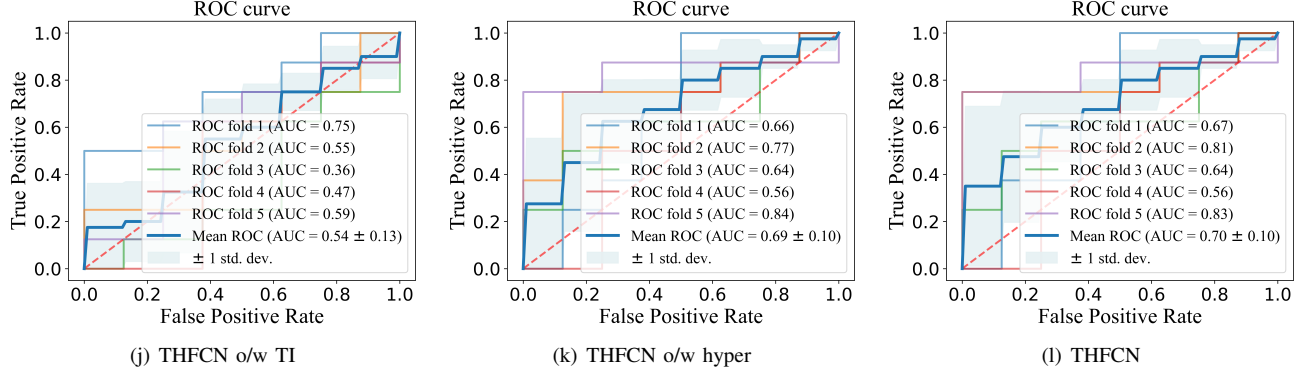
**Fig. S2.** Visualization of  $p$ -values on connections of FCNs between ROIs. (a) The connections with the  $p$ -values less than 0.01. (b) The connections with the  $p$ -values less than 0.005. (c) The connections with the  $p$ -values less than 0.001.



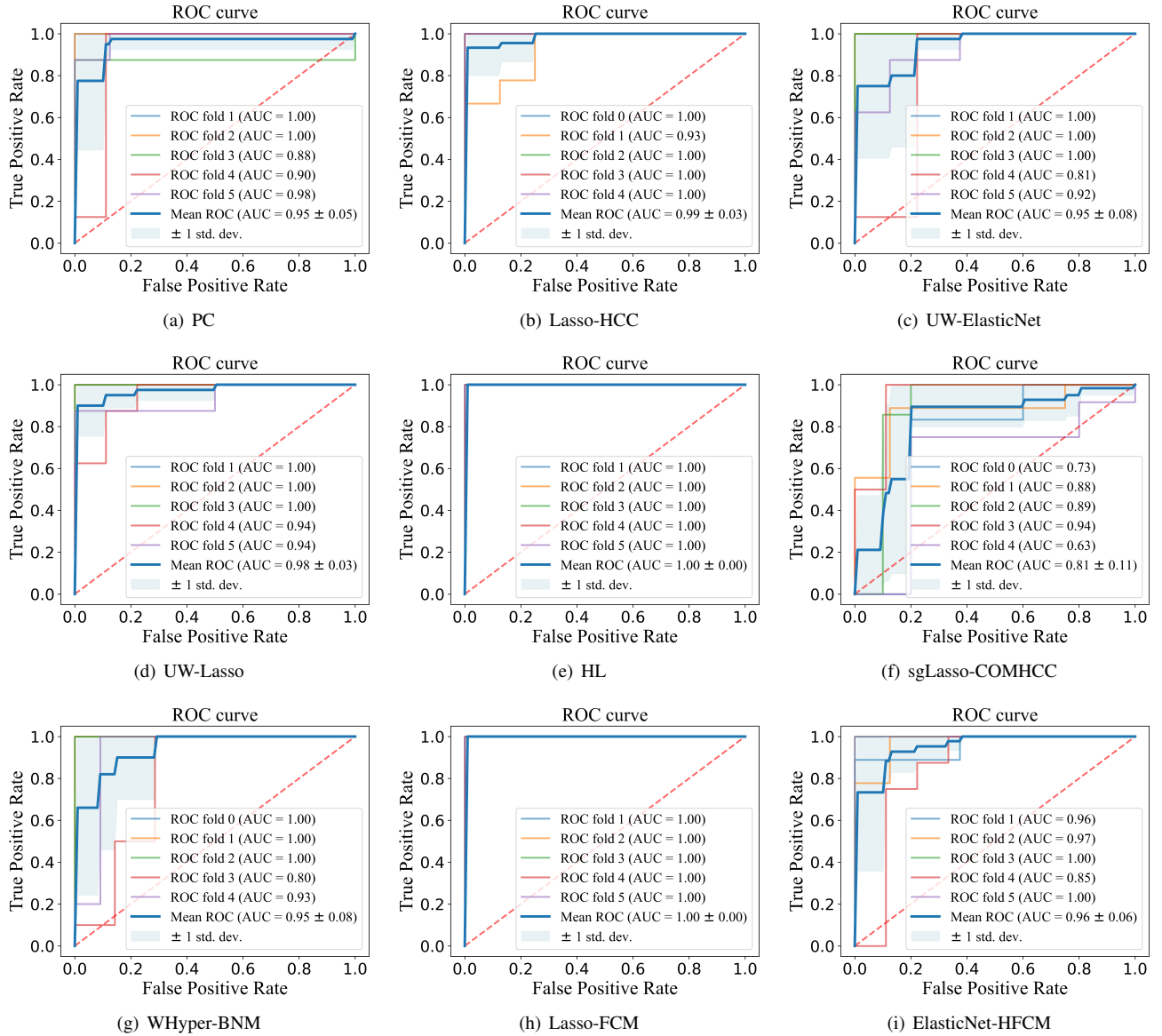


**Fig. S3.** The 5-fold crossover ROC curves of 12 methods on resting-state classified fMRI II data. (a) PC, (b) Lasso-HCC, (c) UW-ElasticNet, (d) UW-Lasso, (e) HL, (f) sgLasso-COMHCC, (g) WHyper-BNM, (h) Lasso-FCM, (i) ElasticNet-HFCM, (j) THFCN o/w TI, (k) THFCN o/w hyper, and (l) THFCN.





**Fig. S4.** The 5-fold crossover ROC curves of 12 methods on Alzheimer's disease fMRI data. (a) PC, (b) Lasso-HCC, (c) UW-ElasticNet, (d) UW-Lasso, (e) HL, (f) sgLasso-COMHCC, (g) WHyper-BNM, (h) Lasso-FCM, (i) ElasticNet-HFCM, (j) THFCN o/w TI, (k) THFCN o/w hyper, and (l) THFCN.



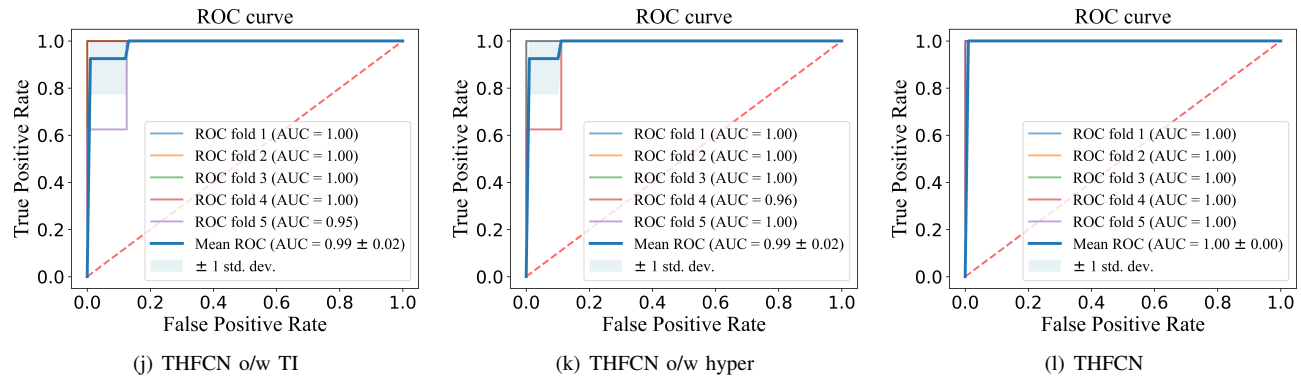


**Fig. S5.** The 5-fold crossover ROC curves of 12 methods on Reading Brain L1 Adult fMRI data. (a) PC, (b) Lasso-HCC, (c) UW-ElasticNet, (d) UW-Lasso, (e) HL, (f) sgLasso-COMHCC, (g) WHyper-BNM, (h) Lasso-FCM, (i) ElasticNet-HFCM, (j) THFCN o/w TI, (k) THFCN o/w hyper, and (l) THFCN.